Journal Pre-proof

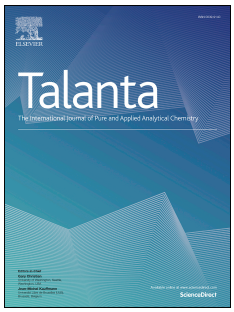

Molybdenum oxide-based metal-organic framework/polypyrrole nanocomposites for enhancing electrochemical detection of dopamine

Kunfeng Zhou, Defeng Shen, Xiao Li, Yuhao Chen, Liran Hou, Yishuai Zhang, Jingquan Sha

PII: S0039-9140(19)31140-3

DOI: https://doi.org/10.1016/j.talanta.2019.120507

Reference: TAL 120507

To appear in: *Talanta*

Received Date: 13 July 2019

Revised Date: 11 October 2019

Accepted Date: 26 October 2019

Please cite this article as: K. Zhou, D. Shen, X. Li, Y. Chen, L. Hou, Y. Zhang, J. Sha, Molybdenum oxide-based metal-organic framework/polypyrrole nanocomposites for enhancing electrochemical detection of dopamine, *Talanta* (2019), doi: https://doi.org/10.1016/j.talanta.2019.120507.

Table of Contents

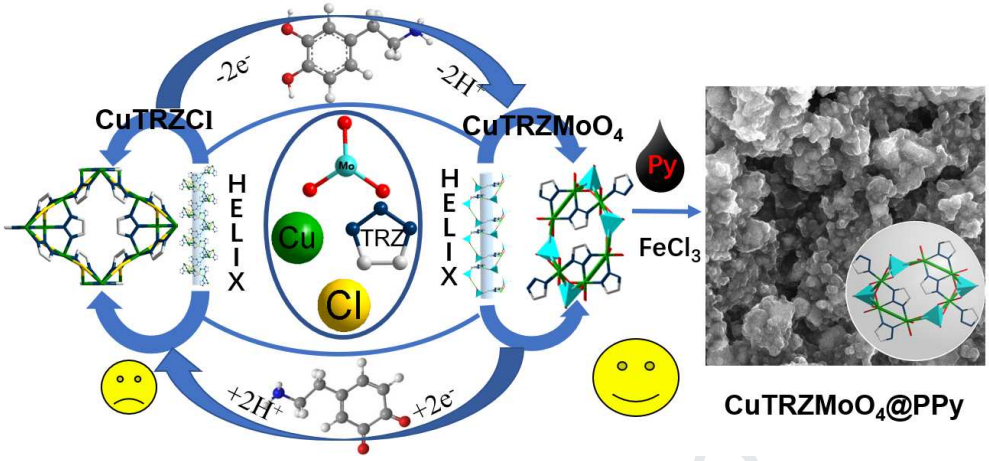

A high active, non-noble MOF based biosensing platform by adjusting the metal centers of MOFs and employing conductive polypyrrole (PPy) for enhancing detection of dopamine (DA) was developed for the first time.

Molybdenum oxide-based Metal-Organic Framework/Polypyrrole Nanocomposites for Enhancing Electrochemical Detection of Dopamine

Kunfeng Zhou,[a,b] Defeng Shen,[b] Xiao Li,[a,b] Yuhao Chen,[a] Liran Hou,[a] Yishuai Zhang,[a] Jingquan Sha[* a]

[a]Department of Chemistry and Chemical Engineering, Jining University, Qufu 273155, P. R. China

[b]School of Pharmacy, Jiamusi University, HeilongJiang, Jiamusi, 154007, P.R. China

*Corresponding author: E-mail address: shajq2002@126.com

Abstract: To overcome the poor conductivities and promote the application in the biosensors of metal-organic frameworks (MOFs), a simple approach was employed to improve their overall conductivity by adjusting the metal centers of MOFs and coating conductive polypyrrole (PPy) in the work. An unprecedented molybdenum oxide-based three-dimensional MOFs with helical channels ($CuTRZMoO_4$) was synthesized based on MoO_4^-, Cu^{2+} ions and 1,2,3-trz for the first time, then combined with PPy to fabricate hybrid composites ($CuTRZMoO_4$@PPy-n) with both advantages. The $CuTRZMoO_4$ modified glassy carbon electrode show high sensitivity for detecting the neurotransmitter dopamine (DA), and the $CuTRZMoO_4$@PPy-2 modified glassy carbon electrode has the highest catalytical activity to DA with the linear detection range from 1 μM to 100 μM and the detection limit of 80 nM (S/N = 3) by differential pulse voltammetry (DPV). Moreover, the developed biosensor has good selectivity,

reproducibility and stability. The concept behinds the new architecture to modify electrodes should promote the further development of MOF-based biosensors.

Keywords: Molybdenum Oxide; Metal-Organic Framework; Polypyrrole; Electrochemical Detection; Dopamine

1. Introduction

Dopamine (DA), one of the most important neurotransmitters, is widely distributed in the brain tissues for message transfer [1, 2]. Generally, abnormal levels of DA can lead to the neurological disorders and various diseases, such as Parkinson's disease, schizophrenia, and others [3]. Therefore, developing a highly sensitive and selective method for the accurate detection of DA is crucial to trace and diagnose diseases. To date, many strategies have been applied to detect DA content, such as HPLC [4], fluorometric [5], electrochemistry etc [6], among which the electrochemical detection has become the mainstream research owing to the sensitive electrochemical oxidation of DA and significant advantages of electrochemistry techniques itself [7, 8]. Unfortunately, DA has a poor response at conventional electrodes owing to sluggish interfacial electron transfer, and coexisting interfering species including uric acid (UA) and ascorbic acid (AA) [9-11]. So, a varieties of materials modified electrodes such as metal nanoparticles [12-14], carbon materials [15], and composites [16] have been proposed for the determination of DA.

Metal–organic frameworks (MOFs) [17] have emerged as powerful platforms for gas storage [18-20], catalysis [21], drug delivery [22-24], sensors [25] and detection [26, 27] owing to their tunable pore sizes, high surface areas, and so on, but insulative nature of most MOFs hinders their electrochemical sensing applications [28]. Polypyrrole (PPy), a class of typical conductive polymer, has received interest in the electrochemical sensing due to environmental stability, good biocompatibility, high surface area [29]. Moreover, attributed to the additional generated electrocatalytic sites, PPy based nanocomposites were also widely explored in the electrochemical detection [30, 31]. So, a simple approach was employed to improve materials overall electrical

conductivity by adjusting the metal centers of MOFs and employing conductive PPy in the work. As far as we know, no correlative research, integrating Mo/Cu based MOFs with PPy for the electrochemical sensor, were reported to date, to the best our knowledge.

Herein, an unprecedented molybdenum oxide-based three dimensional MOFs with helical channels, $[Cu_3(trz)_2(MoO_4)_2]\cdot H_2O$ ($CuTRZMoO_4$), was successfully fabricated by employing the $(NH_4)_6Mo_7O_{24}\cdot 4H_2O$ as molybdenum source and 1,2,3-triazole as organic linker based on the following reasons. Molybdenum exists in three oxidation states (+2, +4, +6), so it can easily participate in redox reactions and exhibit interesting metal conductivity [32-35]. Moreover, the introduction of molybdenum oxide (MoO_3, MoO_4, MoO_5, and MoO_6) into MOFs can obtain new structures with special properties. For comparison, another new MOF, $[Cu_3(trz)_4Cl_2]$ (CuTRZCl), was also reported. Further, to increase the conductivity of $CuTRZMoO_4$, the $CuTRZMoO_4$@PPy-n nanocomposites were fabricated through a chemical oxidation polymerization process of pyrrole *in situ*. The electrochemical response of DA at the $CuTRZMoO_4$@PPy arrays electrode enhances greatly than that of $CuTRZMoO_4$ and CuTRZCl, maybe due to the excessive strong interaction between PPy and $CuTRZMoO_4$, leading to the more electro-catalytical sites, better ion diffusion and faster electron transport.

(Insert Scheme 1)

2. Experimental Section

2.1 Reagent and Instruments

All reagents with the analytical grade were purchased commercially and were used without further purification. Deionized water was used throughout the whole experiment. Phosphate buffer solutions (PBS) were used to investigate the influence of

pH in the 2.0–5.0. Dopamine hydrochloride was obtained from Alpha Chemical Co. Ltd., 1,2,3-triazole was purchased from Aladdin (Shanghai, China). Uric acid (UA), ascorbic acid (AA), D(+)-Glucose (Glc), isopropyl alcohol, pyrrole (Py), alanine (Ala), glutamic glycine (Gly), lysine (Lys), tyrosine (Tyr) were purchased from Sinopharm Chemical Reagical Co. Ltd. (Shanghai, China). Human serum samples were purchased from Hongquan Biotechnology Co., Ltd. (Guangzhou, China).

Elemental analyses for C, H, and N were performed on a Perkin- Elmer 2400 CHN Elemental Analyzer (PerkinElmer, America). The infrared (IR) spectra were performed on an Alpha Centaurt FT/IR spectrometer with KBr pellet in the region of 4000–400 cm^{-1}(Thermo Nicolet Corporation, America). Powder X-ray diffraction (PXRD) patterns were collected on a Rigaku Dmax 2000 X-ray diffractometer with graphite monochromatized Cu-Kα radiation (λ=0.154 nm) and 2θ ranging from 5 to 50° (Rigaku, Japan). X-ray photo-electron spectroscopy (XPS, VG ESCALAB MK II, British) measure were performed on a system with a monochromatized Mg–Kα line scource (1253.6 eV). All binding energies were calibrated by referencing to the C1s peak at 284.6 eV). Raman spectra was measured on a Renishaw micro-Raman spectrometer with 633 nm argon-ion laser as excitation radiation source (Renishaw, British). The morphology and energy dispersive X-ray (EDX) analysis were operated on a scanning electron microscopy (SEM, Phenom ProX, Netherlands) with an accelerating voltage of 15 kV. Electrochemical measurements were performed using a CHI-660C electrochemical workstation (Shanghai Chenhua Instrument Co., Ltd., China) with a conventional three electrode cell.

2.2 Synthesis of $[Cu_3(trz)_2(MoO_4)_2]\cdot H_2O$ ($CuTRZMoO_4$)

The mixture of $(NH_4)_6Mo_7O_{24}\cdot 4H_2O$ (300 mg, 0.24 mmol), $Cu(NO_3)_2$ (150 mg, 0.80 mmol), 1,2,3-trz (60 mg, 0.87 mmol), NH_4VO_3 (36 mg, 0.31 mmol) was dissolved in distilled water (10 mL) with stirring for 0.5 h at room temperature, and pH value was adjusted to 1.8 by $1mol\cdot L^{-1}$ HCl. The resulting solution was transferred into the 20mL Teflon lined stainless steel container and heated at 170°C for 4 days. After the autoclave was cooled to room temperature at 10°C h^{-1}, the green block crystals suitable for X-ray crystallography were obtained, and then washed with distilled water and air-dried (yield: 22% based on Cu). Elemental analysis: $C_4H_6Cu_3Mo_2O_9N_6$ (664.64). Anal. Calcd: H, 0.90; C, 7.22; N, 12.64 (%). Found: H, 1.21; C, 7.17; N, 12.59 (%).

2.3 Synthesis of $[Cu_3(trz)_4Cl_2]$ (CuTRZCl)

The mixture of $Cu(NO_3)_2$ (150 mg, 0.80 mmol), 1,2,3-trz (60 mg, 0.87 mmol), NH_4VO_3 (36 mg, 0.31 mmol) was dissolved in distilled water (10 mL) with stirring for 0.5 h at room temperature, and pH value was adjusted to 1.8 by $1mol\cdot L^{-1}$ HCl. The resulting solution was transferred into the 20 mL Teflon lined stainless steel container and heated at 170°C for 4 days. After the autoclave was cooled to room temperature at 10°C h^{-1}, the green block crystals suitable for X-ray crystallography were obtained, and then washed with distilled water and air-dried (yield: 34% based on Cu). Elemental analysis: $C_8H_8Cu_3Cl_2N_{12}$ (533.77). Anal. Calcd: H, 1.50; C, 18.01; N, 31.51 (%). Found: H, 1.94; C, 17.98; N, 31.34 (%).

2.4 Preparation of the $CuTRZMoO_4$ nanocrystals

Crystal of $CuTRZMoO_4$ were ground for 3 h by physical milling, then the resulting powder was dissolved in methanol and sealed in a Teflon antoclave, and heated in a microwave reactor at 300 W for 4 h. The resulting $CuTRZMoO_4$ nanocrystals were separated by centrifugation, rinsed with water, dried in a vacuum at 80 °C for 24 h.

2.5 Fabrication of $CuTRZMoO_4$@PPy nanocomposites

Pyrrole (Py, 7.5 μL, 1.08×10^{-4} mol) was dissolved in 10 mL deionized water in a beaker. Then $CuTRZMoO_4$ nanocrystals (0.0500 g, 8.24×10^{-5} mol) was placed in the above solution and dispersed supersonically for 0.5 h. 10 ml $FeCl_3$ (0.06 M) solution was slowly added to the above mixture as oxidant. The product was stirred for 10 h, and then left undisturbed for 12 h. The resulting nanocomposites $CuTRZMoO_4$@PPy were separated, subsequently rinsed with water and alcohol, and finally dried at 60 °C in an oven for 24 h. Herein, nanocomposites was prepared in the ratio of [$CuTRZMoO_4$]:[Py] of 1:1 (50 mg : 7.5 μL), 1:2 (50 mg : 15 μL), and 1:4 (50 mg : 30 μL), then the resulting products were labeled as $CuTRZMoO_4$@PPy-1, $CuTRZMoO_4$@PPy-2, and $CuTRZMoO_4$@PPy-3, respectively.

2.6 Preparation and electrochemical measurements of materials modified GCE electrodes

First of all, the GCE was polished with a slurry of alumina oxide powder (1.0, 0.3, and 0.05 μm) to obtain a mirror-like surface. Then the GCE was ultrasonically cleaned in absolute alcohol and distilled water for 2 min and dried by vacuum for further use. The suspension was prepared by mixing MOF or MOF/PPy material (CuTRZCl, $CuTRZMoO_4$, $CuTRZMoO_4$@PPy-n or PPy) 4 mg, 730 μL deionized water and 230 μL polypropanol, and then 40 μL Nafion solution (0.5 wt %) was added to improve the binding strength. Finally, the modified GCE electrode was made by dropping 5 μL catalyst ink on the polished GCE electrode and dried in ambient environment for following measurement. Note that the obtained GCE electrode was rinsed with deionized water and stored in 0.1 M PBS (pH 7.0) prior to be used.

Cyclic Voltammetry (CV) was employed in a PBS solution with 200 and 500 μM DA at a scan rate of 50 mV s^{-1}. Quantitative detection of DA with different concentrations was performed by differential pulse voltammetry (DPV), in which pulse width is 50 ms and the amplitude is 100 mV. Electrochemical impedance spectra (EIS) was employed in a $[Fe(CN)_6]^{3-/4-}$ solution with 0.1 M KCl at a frequency range between 0.01 and 1,000,000 Hz with signal amplitude of 5 mV.

2.7. Real sample preparation

Without any further treatment, 1 mL of human serum sample were deposited in the cell and diluted with 9 mL (0.1 M) PBS at pH 2.5 to be analyzed. Final pH of the solution was 2.55.

2.8 X-ray Crystallographic Study

Crystal data for compounds $CuTRZMoO_4$ and CuTRZCl were collected on Bruker SMART-CCD diffractometer, with Mo-Kα monochromatic radiation (λ = 0.71073 Å) at 293 K. The structure was solved by the direct method and refined full-matrix last squares on F^2 through the SHELXTL and WINGX software package [36]. All non-hydrogen atoms were refined anostropically and the 'ISOR' command was used to refine some ADP problems. Crystal data and structure refinement are listed in Table S1. Selected bond lengths and angles are listed in Table S2. CCDC number 1817883 for $CuTRZMoO_4$ and 1911580 for CuTRZCl.

3. Results and discussion

3.1 Structural description of $CuTRZMoO_4$ and CuTRZCl

Single crystal X-ray diffraction analysis shows the asymmetric unit and fabrication mode of $CuTRZMoO_4$ are shown in support information Fig. S1a and S1b, and the results of the valence sum calculations about metal ions are listed in Table S3 [37-39].

$CuTRZMoO_4$ exhibits a complicated 3D MOFs consisting of 2D MoO_4-Cu inorganic layer and 1D Cu-trz chains. More specifically, two trz ligand adopting imidazole-like coordination modes link with two Cu1 ions forming $[Cu_2(trz)_2]^{2+}$ subunit, then each such $[Cu_2(trz)_2]^{2+}$ subunits connect each other forming a 1D organic-inorganic hybrid chain *via* Cu2 ions (Fig. 1a). On the other hand, each MoO_4 anion as four dentate inorganic ligands coordinate with five Cu ions (three Cu1 and two Cu2) (Fig. S1c) fabricating the 2D inorganic sheet (Fig. 1b). Finally, the 2D inorganic layer is cross-linked with a 1D organic chain forming the whole 3D framework by sharing Cu1 and Cu2 ions (Fig. 1c). From the topological view, $CuTRZMoO_4$ exhibits an unique (4,5)-connected 3D framework with $\{4^3\cdot6^2\cdot8\}^2\{4^4\cdot6^2\}\{4^5\cdot6^5\}^2$ topology. In this simplification, the 4-connected nodes are Cu1 and Cu2 ions, and the 5-connected nodes are MoO_4 anion (Fig. 1d and S2a). It is interesting that there is one kind of meso- helical channel structure. As shown in Fig. 1e, MoO_4 anion, $[Cu_2(trz)_2]^{2+}$ subunits and Cu2 ion are alternately connected to fabricate left- and right-handed helical chains with the pitch of screw of 11.070 Å along *b* axis *via* the Cu2-MoO_4-Cu1-Cu1-MoO_4-Cu2-MoO_4-Cu1-Cu1-MoO_4. Afterwards, the left- and right-handed helical chains connect each other by sharing MoO_4-Cu forming 1D tunnel, which is occupied by coordinated trz ligands (Figs. S2b and S3). Compound CuTRZCl also exhibits a complicated 3D MOFs, but the fabrication mode is different from $CuTRZMoO_4$, and detailed structure descriptions can be found in support information (Fig. S4-S7).

(Insert Figure 1)

3.2 PXRD, FT-IR, Raman, XPS, EDX and SEM characterization of materials

Both simulated and experimental PXRD patterns match well revealing the phase purity of compounds CuTRZCl and $CuTRZMoO_4$ (Fig. S8). PXRD pattern of

$CuTRZMoO_4$@PPy-n (n=1, 2 and 3) exhibit similar diffraction patterns to that of corresponding matrix, illustrating the structural integrality during the polymerization of Py (Fig. 2a). Note that there were no noticeable characteristic peaks of PPy in $CuTRZMoO_4$@PPy-n implying a good dispersion and small amount of PPy. The FT-IR spectra of PPy, CuTRZCl, $CuTRZMoO_4$ and $CuTRZMoO_4$@PPy-n (n=1, 2 and 3) were recorded and represented in Fig. S9. The characteristic peaks at 942, 840, 822 and 723 cm^{-1} are attributed to ν(Mo-O-Cu) vibrations, respectively. Band in the region of 1605-1123 cm^{-1} are attributed to the trz ligand. These characteristic peaks at *ca.* 1039, 1331 and 1548 cm^{-1} in $CuTRZMoO_4$@PPy-n are ascribed to the stretching vibrations of pyrrole ring groups [40-42]. Raman spectra of $CuTRZMoO_4$ and $CuTRZMoO_4$@PPy-2 (λ_{ex} = 633 nm) also presents characteristic bands of PPy at 1320 and 1586 cm^{-1}, which are responsible for the C–N and C=C stretching [43, 44], respectively, confirming the presence of PPy (Fig. 2b). X-ray photoelectron spectrum (XPS) of $CuTRZMoO_4$@PPy-2 shows the coexistence of C, N, O, Cu and Mo elements shown in Fig. 2c-h. More specifically, two Gaussian peaks related with C-C/C=C, and C-N/C=N (284.4, and 286.6 eV respectively) were observed. The N1s spectrum (pyrrolic-N, *ca.* 399 eV), being divided into three peaks ascribed to –N= and –NH– segments (398.8 and 399.8 eV) in the backbone of PPy chains, while the peak at 400.8 eV belongs to the protonation states ($-NH^+-$). Two peaks at 933.5 eV and 955.4 eV may attribute to Cu^{2+} $2p_{3/2}$ and Cu^{2+} $2p_{1/2}$, respectively. And Mo 3d spectrum exhibits two main peaks at 232.3 eV of Mo^{6+} $3d_{3/2}$ and 235.4 eV of Mo^{6+} $3d_{5/2}$ [45-47]. Moreover, the morphology of CuTRZCl, $CuTRZMoO_4$ and $CuTRZMoO_4$@PPy-n were investigated by the scanning electron microscopy (SEM) (Fig. S10). It is obvious that $CuTRZMoO_4$@PPy-n (n=1, 2 and 3) shows a coarse, irregular surface and circular fringe owing to the

wrapping of PPy, which indicates that PPy has been successfully coated on the surface of $CuTRZMoO_4$. In addition, the EDS spectra (Fig. S11-S13) indicate the homogenous distribution of C, O, N, Cu and Mo/Cl elements in CuTRZCl, $CuTRZMoO_4$ and $CuTRZMoO_4$@PPy-n, respectively.

(Insert Figure 2)

3.3 Electrochemical performances of as-prepared sample modified electrodes

As we all know that the electrochemical behavior of DA has been proposed to occur *via* the electron transport-chemical reaction-electron transfer (ECE) mechanism [48], and the reaction of oxidized DA is divided into two steps shown in Scheme S1. Herein, the electrochemical performance of the as-prepared samples modified electrodes were explored by cyclic voltammetry (CV), in which the electrodes are bare GCE, PPy/GCE, CuTRZCl/GCE, $CuTRZMoO_4$/GCE, $CuTRZMoO_4$@PPy-n/GCE (n=1, 2 and 3). As shown in Fig. 3a, all CV curves display a pair of redox peaks at *ca*.0.5 V of $E_{1/2} = (E_{pc} + E_{pa})/2$ in 0.1M PBS solution (pH 2.5) containing 0.2 mM DA, corresponding to DA oxidation to DAQ and DAQ back to DA, respectively. Obviously, compared to the bare GCE, the oxidation current of DA had a considerable increase after modified by $CuTRZMoO_4$, maybe due to the activity of $CuTRZMoO_4$ supplying multiple metal site and increasing the electrode/electrolyte interface [49, 50]. Once PPy is introduced, the oxidation current of DA further increases and the peak separation ΔE_p($\Delta E_p = E_{pa}-E_{pc}$) decreases from 230 mV to 204 mV in $CuTRZMoO_4$@PPy-n/GCE (n=1, 2 and 3) (Table S4), maybe due to the increasing specific surface area and a smart microenvironment for the movement of DA towards active centers by the addition of PPy. Meanwhile, to identity the role of hybrid of PPy and Mo/Cu based MOFs, we also tested the electrochemical performance of PPy and CuTRZCl modified GCE, and the CV curves

show no obvious electrochemical response. In addition, when keeping the same reaction condition, the higher the loading amount is, the higher oxidation current is, however the increasing trend becomes slowly. So $CuTRZMoO_4$@PPy-2/GCE is chose for the subsequent analytical assay. The above results togerther verify that the hybrid of PPy and $CuTRZMoO_4$ could induce faster charge transfer kinetics in $CuTRZMoO_4$@PPy-n/GCE (n = 1, 2, and 3) [51].

Many factors including pH of buffer solution can affect the current response for the DA detection, so the influence of pH on the detecting DA current response of $CuTRZMoO_4$@PPy-2 were explored by employing the CV test in 0.1 M PBS containing 0.2 mM DA pH ranging from 1.0 to 5.0. As shown in Fig. 3b, the oxidation peak potential shift negatively when the pH value increase from 1.0 to 5.0, indicating that protons participate in the electrode reaction [52, 53]. Because the oxidation peak current reaches the maximum value at pH 2.5, pH 2.5 (0.1 M) PBS is chosen as the best reaction condition for the subsequent analytical assay.

(Insert Figure 3)

To further study the dynamics of MOFs modified electrode, the electrochemical impedance spectroscopy (EIS) was studied shown in Fig. 4a. It is obvious that the diameter of semi-circle of bare GCE is significantly larger than those of the others in high frequency region, and that of $CuTRZMoO_4$@PPy-2/GCE is the smallest. The fact indicates the $CuTRZMoO_4$@PPy-2/GCE modified electrode can provide the fastest charge transfer rate among all as-prepared electrodes maybe due to the introduction of PPy, which were consistent with the above analysis from CV. Moreover, the scan rate dependent CV on $CuTRZMoO_4$@PPy-2/GCE was also investigated in 0.5 mM DA solution in the range of 50-500 mVs^{-1}. The linear equations follow as:

i_{pa} (μA) = 42.95+7.71$v^{1/2}$ $(mV/s)^{1/2}$, R_2 = 0.994,

i_{pc} (μA) = -19.68-3.28 $v^{1/2}$ $(mV/s)^{1/2}$, R_2 = 0.991.

A positive shift of anodic peak potential (correspondingly, a negative shift of cathodic peak potential) with increasing *v* was observed (Fig. 4b), and good linear relationship between peak currents (i) and square root of the scan rate ($v^{1/2}$) indicated a typical diffusion controlled process.

(Insert Figure 4)

As we know that the sensing performance of DA oxidation processes is believed to occur on the electrode surface, so the response of CuTRZMoO$_4$@PPy-2/GCE electrode to DA was studied by differential pulse voltammetry (DPV) at pH 2.5 (0.1 M PBS solution). With the increasing of DA concentration, the current are significantly increased, and exhibit a good linear response (correlation coefficient is 0.990) in the range of 1 μM to 100 μM (Fig. 5a). The linear formula of CuTRZMoO$_4$@PPy-2/GCE is i_p(μA) = 1.6145+0.1988c, and the limit of detection (LOD) was calculated as 80 nM (S/N = 3) (LOD=KS_0/*S*, where K is a numerical factor determined by the desirable confidence level, S_0 is the standard deviation (SD) of the blank measurements (n = 10, K = 3), and *S* is the slope of the calibration curve). The LOD value is lower than other reported modified electrodes, implying that CuTRZMoO$_4$@PPy-2/GCE have the superiority for the electrochemical sensing of DA (Table 1). This fact may be attributed to the large surface area, abundant active sites and good conductivity of the CuTRZMoO$_4$@PPy-2 composite, which are essential for improving the electrochemical activity. In addition, the stability and reproducibility of CuTRZMoO$_4$@PPy-2/GCE sensor for detecting DA were explored by CV, and the oxidant peak current of DA was *ca* 90% and 87% of the initial value after 100 cycles of continuous scanning and one

week, respectively, indicating the good electrode stability (Fig. S14), whihc attribute to the stronger affinity between the PPy sheet and intriguing 3D MOFs. Meanwhile, five groups of relatively independent $CuTRZMoO_4$@PPy-2/GCE electrodes were prepared and used to detect 0.2 mM DA, the result show that the relative standard deviation (RSD) was 3.8 %.

(Insert Figure 5)

(Insert Table 1)

To evaluate the selectivity of $CuTRZMoO_4$@PPy-2 modified-GCE for DA, an investigation about the influence of potential interfering substances in human body, including alanine (Ala), glycine (Gly), lysine (Lys), tyrosine (Tyr), glucose(Glc), ascorbic acid(AA), uric acid (UA), and 4 kinds of ions (Na^+, Ca^{2+}, K^+, and Cl^-), was performed under the optimized conditions. Fig. 5b shows the DPV responses upon addition of interfering substances into 0.1 M PBS (pH 2.5), respectively (UA and DA at a concentration of 100 μM and other substances at a concentration of 1000 μM). It is found that DA exhibits an obvious anodic current response at Ep_{DA} peak, although the concentrations of others reach ten times of DA. This results suggest that the $CuTRZMoO_4$@PPy-2 modified-GCE sensor has the excellent selectivity to DA.

The anti-interference ability of DA detections can be demonstrated by performing two types of experiments. More specifically, the different potential interfering compounds at the $CuTRZMoO_4$@PPy-2 modified-GCE was studied under the optimum conditions in a solution containing 50.0 μM of DA in 0.1 M PBS (pH 2.5) by using DPV. As shown in Fig. 6a and Table S5, 20-fold of alanine (Ala), glycine (Gly), lysine (Lys), tyrosine (Tyr), glucose (Glc), ascorbic acid (AA), Na^+, Ca^{2+}, K^+, and Cl^-, and 1-fold of uric acid (UA) do not affect the anti-interference ability of DA detection.

Because the peak of UA has a potential interference, and a second set of experiment was performed to rule out this effect. The concentration of DA was fixed while the UA concentration was changed from 20 μM to 160 μM (Fig. 6b and Table S6), and the corresponding peaks were completely separated, and the current-change values ranged from -0.954% to +2.796% in comparison with its initial values, indicating that UA did not produce significantly influence in the determination DA. Collectively, the $CuTRZMoO_4$@PPy-2 modified-GCE exhibits high anti-interference ability for DA detection.

(Insert Figure 6)

In final, the application of $CuTRZMoO_4$@PPy-2/GCE as sensor for the detection DA in the real samples such as human serum is measured. The recovery of DA was studied by spiking test samples with four different concentrations. After spiking four groups of standard DA solutions with different concentrations (1, 10, 50 and 100 μM) in 10-fold diluted samples, as shown in Table 2. The results show that the recoveries of DA for different human serum are 103, 101.3, 99.34 and 100.18%, and the RSDs for five successive measurements were below 5%. These results clearly demonstrate the potential applications of the $CuTRZMoO_4$@PPy-2/GCE sensor in clinical determination of DA.

(Insert Table 2)

4. Conclusions

In short, two new MOF materials, $CuTRZMoO_4$ and CuTRZCl, were successfully synthesized and characterized. The $CuTRZMoO_4$ electrode exhibited the better catalytic activity toward oxidation of DA than that of CuTRZCl, maybe due to the higher oxidation state of molybdenum providing more electron transfer. By effectively

combining $CuTRZMoO_4$ and PPy, a high active DA sensor, $CuTRZMoO_4$@ppy-2 ($CuTRZMoO_4$: Py ratio is 50 mg : 15 μl), is obtained. The as-prepared $CuTRZMoO_4$@ppy-2 electrode presented stronger DA activity, the satisfactory stability and selectivity with a linear detection range of 1 μM to 100 μM and the low detection limit of 80 nM, owing to the addition of appropriate surface area and the synergistic effect of components. The availability of molybdenum oxide-based MOFs combined with PPy could be widely used in the practical measurement of DA detection.

Acknowledgements

Financial support from the Talent Culturing Plan for Leading Disciplines and the Natural Science Foundation (ZR2017LB001) of Shandong Province.

References

[1] J, Yang, Y. Hu, Y. Li, Molecularly imprinted polymer-decorated signal on-off ratiometric electrochemical sensor for selective and robust dopamine detection，Biosens. Bioelectron. 135 (2019), 224-230.

[2] M. S. Hsu, Y.L. Chen, C. Y. Lee, and H. T. Chiu, Gold Nanostructures on Flexible Substrates as Electrochemical Dopamine Sensors, ACS applied materials & interfaces 4 (2012), 5570-5575.

[3] S. Demuru, L. Nela, N. Marchack, S. J. Holmes, D. B. Farmer, G. S. Tulevski, Q. Lin H. Deligianni, Scalable nanostructured carbon electrode arrays for enhanced dopamine detection, ACS sensors 3 (2018), 799-805.

[4] V. Carrera, E. Sabater, E. Vilanova, M. A. Sogorb, A simple and rapid HPLC–MS method for the simultaneous determination of epinephrine, norepinephrine, dopamine and 5-hydroxytryptamine: Application to the secretion of bovine chromaffin cell cultures, Journal of Chromatography B 847 (2007), 88-94.

[5] Y. Tao, Y. Lin, J. Ren X. Qu, Gold Nanostructures on Flexible Substrates as Electrochemical Dopamine Sensors, Biosens. Bioelectron. 42 (2013), 41-46.

[6] C. Xue, Q. Han, Y. Wang, J. Wu, T. Wen, R. Wang, J. Hong, X. Zhou, H Jiang, Amperometric detection of dopamine in human serum by electrochemical sensor based on gold nanoparticles doped molecularly imprinted polymers, Biosens. Bioelectron. 49 (2013), 199-203.

[7] T. Qian, C. Yu, X. Zhou, P. Ma, S. Wu, L. Xu, J. Shen, Amperometric detection of dopamine in human serum by electrochemical sensor based on gold nanoparticles doped molecularly imprinted polymers, Biosens. Bioelectron. 58 (2014), 237-241.

[8] Y. Li, J. Liu, M. Liu, F. Yu, L. Zhang, H. Tang, B. C. Ye, L. Lai, Fabrication of ultra-sensitive and selective dopamine electrochemical sensor based on molecularly imprinted polymer modified graphene@carbon nanotube foam Electrochem. Commun. 64 (2016), 42-45.

[9] C. R. Raj, T. Ohsaka, Electroanalysis of ascorbate and dopamine at a gold electrode modified with a positively charged self-assembled monolayer, Journal of Electrochem. Commun. 496 (2001), 44-49.

[10] F. Malem, and D. Mandler, Self-Assembled Monolayers in Electroanalytical Chemistry: Application of w-Mercapto Carboxylic Acid Monolayers for the Electrochemical Detection of Dopamine in the Presence of a High Concentration of Ascorbic Acid, Anal. Chem. 65 (1993), 37-41.

[11] X. Zheng, Y. Guo, J. Zheng, X. Zhou, Q. Li, R. Lin, Simultaneous determination of ascorbic acid, dopamine and uric acid using poly(L-leucine)/DNA composite film modified electrode, Sensors and Actuators B: Chemical. 213 (2015), 188-194.

[12] C. Zhou, S. Li, W. Zhu, H. Pang, H. Ma, A sensor of a polyoxometalate and Au–Pd alloy for simultaneously detection of dopamine and ascorbic acid, Electrochimica Acta 113 (2013), 454-463.

[13] Y. Zheng, Z. Huang, C. Zhao, S. Weng, W. Zheng X. Lin, A gold electrode with a flower-like gold nanostructure for simultaneous determination of dopamine and ascorbic acid, Microchimica Acta 180 (2013), 537-544.

[14] Y. Zhao, S. H. Lia, J. Chu, Y. P. Chen, W. W.Lia, H. Q. Yu, G. Liu, Y. C. Tian, Y. Xiong, A nano-sized Au electrode fabricated using lithographic technology for Electrochemical detection of dopamine, Biosens. Bioelectron. 35 (2012), 115-122.

[15] T. Qian, S. Wu, J. Shen, Facilely prepared polypyrrole-reduced graphite oxide core-shell microspheres with high dispersibility for electrochemical detection of dopamine, Chem. Commun. 49 (2013), 4610-4612.

[16] Q. Huang, H. Zhang, S. Hu, F. Lia, W. Weng, J. Chen, Q. Wang, Y. He, W. Zhang, X. Bao, A sensitive and reliable dopamine biosensor was developed based on the Au@carbon dots-chitosan composite film, Biosens. Bioelectron. 52 (2014), 277-280.

[17] S. T. Meek, J. A. Greathouse, M. D. Allendorf, Metal□organic frameworks: A rapidly growing class of versatile nanoporous materials, Adv.Mater. 23 (2011), 249.

[18] K. Sumida, D. L. Rogow, J. A. Mason, T. M. McDonald, E. D. Bloch, Z. R. Herm, T. H. Bae, J. R. Long, Carbon dioxide capture in metal-organic frameworks, Chem. Rev. 112(2011), 724-781.

[19] J. Park, L. B. Sun, Y. P. Chen, Z. Perry, H. C. Zhou, Azobenzene□Functionalized Metal-Organic Polyhedra for the Optically Responsive Capture and Release of Guest Molecules. Angew. Chem. Int. Ed. 53 (2014), 5842.

[20] J. Y. Lee, L. Pan, S. P. Kelly, J. Jagiello, T. J. Emge, J. Li, Achieving high density of adsorbed hydrogen in microporous metal organic frameworks, Adv. Mater. 17 (2005), 2703.

[21] J. Lee, O. K. Farha, J. Roberts, K. A. Scheidt, S. T. Nguyenand, J. T. Hupp, Metal-organic framework materials as catalysts, Chem. Soc. Rev. 38 (2009), 1450.

[22] P. Horcajada, C. Serre, M. Vallet□Regí, M. Sebban, F. Taulelle, G. Férey, Metal-organic frameworks as efficient materials for drug delivery, Angew. Chem. Int. Ed. 45 (2006), 5974.

[23] J. An, S. J. Geib, N. L. Rosi, Cation-triggered drug release from a porous zinc-adeninate metal-organic framework, J. Am. Chem. Soc. 131 (2009), 8376.

[24] R. Ananthoji, J. F. Eubank, F. Nouar, H. Mouttaki, M. Eddaoudi, J. P. Harmon, Symbiosis of zeolite-like metal-organic frameworks (rho-ZMOF) and hydrogels: Composites for controlled drug release, J. Mater. Chem. 2011, 21 (2011), 9587.

[25] L. E. Kreno, K. Leong, O. K. Farha, M. Allendorf, R. P. Van Duyne, J. T. Hupp, Metal-organic framework materials as chemical sensors, Chem. Rev. 112 (2012), 1105.

[26] Y. Guo, X. Feng, T. Han, S. Wang, Z. Lin, Y. Dong, B. Wang, Tuning the luminescence of metal-organic frameworks for detection of energetic heterocyclic compounds, J. Am. Chem. Soc. 136 (2016), 15485.

[27] H. Li, X. Feng, Y. Guo, D. Chen, R. Li, X. Ren, X. Jiang, Y. Dong, B. Wang, A malonitrile-functionalized metal-organic framework for hydrogen sulfide detection and selective amino acid molecular recognition, Sci. Rep. 4 (2014), 4366.

[28] J. Li, J. Xia, F. Zhang, Z. Wang, Q. Liu, A Novel Electrochemical Sensor Based on Copper-based Metal-Organic Framework for the Determination of Dopamine, Journal of the Chinese Chemical Society 65 (2018), 743-749.

[29] M. Lin, M. S. Cho, W. S. Choe, J. B. Yoo, Y. Lee, Polypyrrole nanowire modified with Gly-Gly-His tripeptide for electrochemical detection of copper ion, Biosens. Bioelectron. 26 (2010), 940-945.

[30] F. Wang, L. Zhu and J. Zhang, Sensors and Actuators B: Chemical., 2014, 192, 642-647.

[31] K. Xue, S. Zhou, H. Shi, X. Feng, H. Xin, W. Song, Electrochemical sensor for levofloxacin based on molecularly imprinted polypyrrole–graphene–gold nanoparticles modified electrode, Sensors and Actuators B: Chemical 203 (2014), 412-416.

[32] G. Schwarz, R. Mendel, M. W. Ribbe, Molybdenum cofactors, enzymes and pathways, Nature 460 (2009), 839.

[33] H. Zhang, Y. Wang, E. R. Fachini, C. R. Cabrera, Electrochemically codeposited platinum/molybdenum oxide electrode for catalytic oxidation of methanol in acid solution, Electrochemical and solid-state letters 2 (1999), 437-439.

[34] A. B. Lysenko, G. A. Senchyk, J. Lincke, D. Lässig, A. A. Fokin, E. D. Butova, P. R. Schreiner, H. Krautscheid, K. V. Domasevitch, Metal oxide-organic frameworks (MOOFs), a new series of coordination hybrids constructed from molybdenum (VI) oxide and bitopic 1, 2, 4-triazole linkers, Dalton Trans. 39 (2010), 4223-4231.

[35] E. Fazio, S. Spadaro, M. Bonsignore, N. Lavanya, C. Sekar, S.G. Leonardi, G. Neri, F. Neri, Molybdenum oxide nanoparticles for the sensitive and selective detection of dopamine, Journal of Electroanalytical Chemistry 814 (2018), 91-96.

[36] (a) G. M. Sheldrick, SHELX-97, Program for Crystal Structure Refinement, University of Göttingen, Germany, 1997; (b) G. M. Sheldrick, SHELXL-97, Program for Crystal Structure Solution, University of Göttingen, Germany, 1997.

[37] I. D. Brown, D. Altermatt, Bond-valence parameters obtained from a systematic analysis of the inorganic crystal structure database, Acta Crystallographica Section B: Structural Science 41 (1985), 244-247.

[38] N. E. Brese, M. O'keeffe, Bond-valence parameters for solids, Acta Crystallographica Section B: Structural Science 47 (1991), 192-197.

[39] I. D. Brown, Recent developments in the methods and applications of the bond valence model, Chemical Reviews 109 (2009), 6858-6919.

[40] H. Eshtiagh-Hosseinia, M. R. Housaindokht, S. A. Beyramabadi, S. H. M. Tabatabaei, A. A. Esmaeili, M. J. Khoshkholgh, Synthesis, experimental and theoretical characterization of N, N′-dipyridoxyl (1, 4-butanediamine) Schiff-base ligand and its Cu (II) complex, Spectrochimica Acta Part A: Molecular and Biomolecular Spectroscopy 78 (2011), 1046-1050.

[41] Z. Neisi, Z. Ansari-As, S. Jafarinejad-Farsangi, M. E. Tarzi, T. Sedaghat, V. Nobakht, Synthesis, characterization and biocompatibility of polypyrrole/Cu (II) metal-organic framework nanocomposites, Colloids and Surfaces B: Biointerfaces 178 (2019), 365-376.

[42] A. Sobhani-Nasab, S. Behvandi, M. A. Karimi, E. Sohouli, M. S. Karimi, N. Gholipour, F. Ahmadi, M. Rahimi-Nasrabadi, Synergetic effect of graphene oxide

and C_3N_4 as co-catalyst for enhanced photocatalytic performance of dyes on $Yb_2(MoO_4)_3/YbMoO_4$ nanocomposite, Ceramics International 2019.

[43] N. Su, H. B. Li, S. J. Yuan, S. P. Yi, E. Q. Yin, Synthesis and characterization of polypyrrole doped with anionic spherical polyelectrolyte brushes, Express Polymer Letters, 6 (2012).

[44] Y. Jiao, G. Chen, D. Chen, J. Pei, Y. Hu, Bimetal-organic framework assisted polymerization of pyrrole involving air oxidant to prepare composite electrodes for portable energy storage, J. Mater. Chem. A. 5 (2017), 23744-23752.

[45] H. N. Wang, M. Zhang, A. M. Zhang, F. C. Shen, X. K. Wang, S. N. Sun, Y. J. Chen, Y. Q. Lan, Polyoxometalate-Based Metal-Organic Frameworks with Conductive Polypyrrole for Supercapacitors, ACS applied materials & interfaces 10 (2018), 32265-32270.

[46] X. Li, L. Sun, X. Yang, K. Zhou, G. Zhang, Z. Tong, C. Wang, J. Sha, Enhancing the colorimetric detection of H_2O_2 and ascorbic acid on polypyrrole coated fluconazole-functionalized POMOFs, Analyst 144 (2019), 3347-3356.

[47] J. G. Choi, L. T. Thompson, XPS study of as-prepared and reduced molybdenum oxides, Applied Surface Science 93 (1996), 143-149.

[48] L. A. Mercante, A. Pavinatto, L. E. O. Iwaki, V. P. Scagion, V. Zucolotto, O. N. O. Jr., L. H. C. Mattoso, D. S. Correa, Electrospun polyamide 6/poly (allylamine hydrochloride) nanofibers functionalized with carbon nanotubes for electrochemical detection of dopamine, ACS applied materials & interfaces 7 (2015), 4784-4790.

[49] H. N. Miras, J. Yan, D. L. Long, L. Cronin, Engineering polyoxometalates with emergent properties, Chemical Society Reviews 41(2012), 7403-7430.

[50] J. D. Compain, K. Nakabayashi, S. Ohkoshi, A polyoxometalate-cyanometalate multilayered coordination network, Inorg. Chem 51 (2012), 4897-4899.

[51] L. A. Mercante, A. Pavinatto, L. E. O. Iwaki, V. P. Scagion, V. Zucolotto, O. N. OliveiraJr, L. H. C. Mattoso, D. S. Correa, Electrospun polyamide 6/poly (allylamine hydrochloride) nanofibers functionalized with carbon nanotubes for electrochemical detection of dopamine, ACS applied materials & interfaces 7 (2015), 4784-4790.

[52] W. Zhang, G. Jia, Zh. Li, C. Yuan, Y. Bai, D. Fu, Selective Electrochemical Detection of Dopamine on Polyoxometalate□Based Metal-Organic Framework and Its Composite with Reduced Graphene Oxide, Advanced Materials Interfaces 4 (2017), 1601241.

[53] E. Nagles, L. Ibarra, J. P. Llanos, J. Hurtado, O. Garcia-Beltrán, Development of a novel electrochemical sensor based on cobalt (II) complex useful in the detection of dopamine in presence of ascorbic acid and uric acid, Journal of Electroanalytical Chemistry 788 (2017), 38-43.

[54] H. Yang, D. Liu, X. Zhao, J. H. Yang, H. Chang, R. Xing, S. Liu, AuPd bimetallic nanoparticle-supported carbon nanotubes for selective detection of dopamine in the presence of ascorbic acid, Analytical Methods 9 (2017), 3191-3199.

Table 1. Comparison of Composition, Detection Limit and Linear Range of Different Modified Electrodes for Determination of DA.

Matrix	Materials	Methods	Linear range (μM)	LOD (μM)	Sample analysis	Ref
0.1 MPBS (pH 6.5)	PPy/CNTs-MIPs	DPV	5.0×10^{-5}-5.0	1.0×10^{-4}	Serum	[7]
PBS (pH 7.0)	graphene@carbon nanotube	CV	2×10^{-9}-1×10^{-6}	6.67×10^{-10}	—	[8]
0.2 MPBS (pH 7.0)	Au–Pd alloy	DPV	1.2-1610	0.43	serum	[12]
0.1 MPBS (pH 6.0)	Cu-MOF	DPV	0.5-100	0.15	injection	[28]
0.01 MPBS (pH 7.0)	PA6/PAH_MWCNTs	DPV	1.0-70	0.15	—	[51]
0.1 MPBS (pH 7.0)	POMOF/rGO	DPV	1.0-200	0.0804	serum	[52]
0.001 M PBS(pH 2.0)	N-SWCNT $[Co(bdmpzm)_2(NCS)_2]$/SPCE	SWV	0.62-5.56	0.095	urine	[53]
0.1 MPBS (pH 7.0)	AuPd/CNTs	DPV	0.2-50	0.083	urine	[54]
0.1 M PBS(pH 2.5)	$CuTRZMoO_4$/PPy nanocomposite	DPV	1-100	0.080	serum	This work

Table 2. Detection of dopamine in 10% human serum samples.

Samples	Amounts of added DA (μM)	Amounts of found DA (μM)	Recovery (%)	RSD (%)
10% Human serum	1	1.03	103	1.47
10% Human serum	10	10.13	101.3	0.96
10% Human serum	50	49.67	99.34	1.13
10% Human serum	100	100.18	100.18	3.26

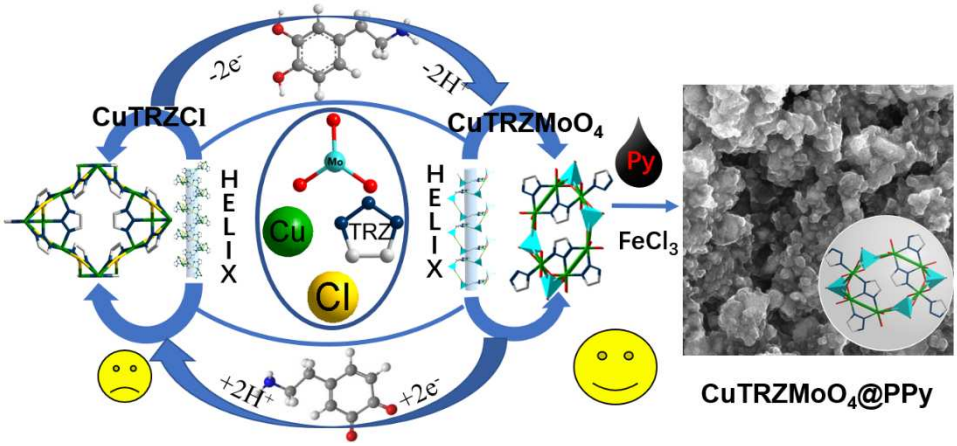

Scheme 1. Schematic illustration of the synthetic process of MOFs and MOFs@PPy as an enhancing electrochemical biosensing platform.

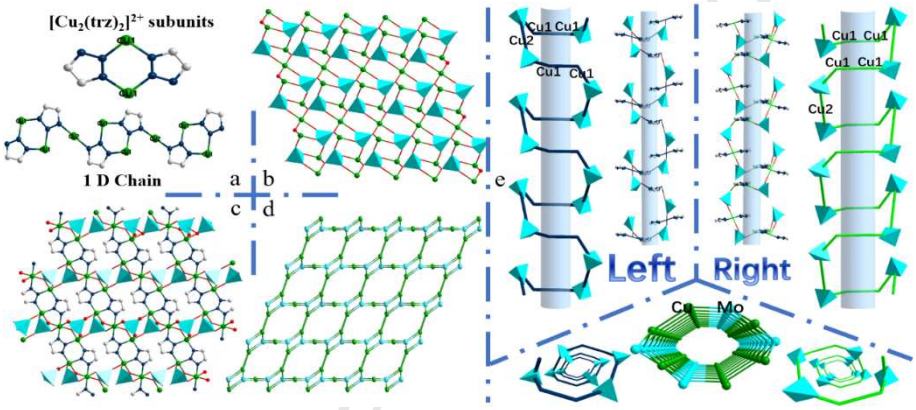

Fig. 1. (a) Ball/stick representation of 1D inorganic-organic hybrid chain, (b) 2D inorganic layer, (c) 3D framework and (d) topological structure; (e) View and schematic representation of the left- and right-handed helical chains constructed from Cu ions,$[Cu_2(trz)_2]^{2+}$ subunits and MoO_4 anion along b axis.

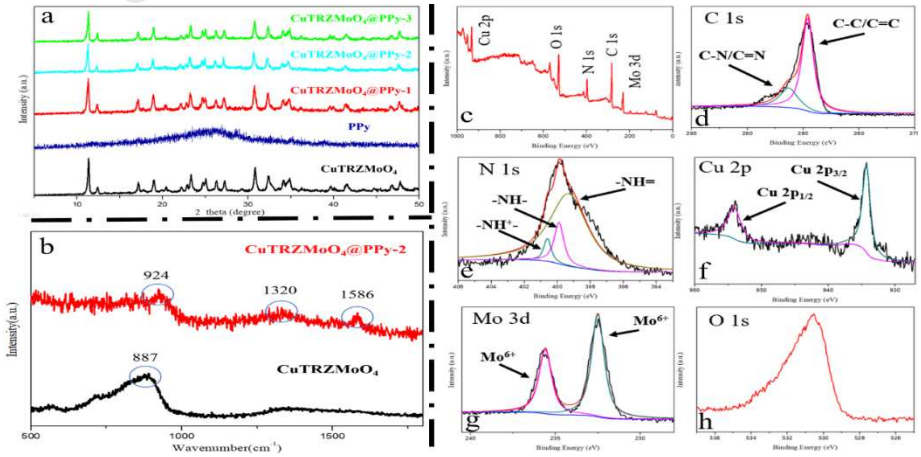

Fig. 2. (a) Characterization of the as-prepared samples (CuTRZCl, $CuTRZMoO_4$, PPy and $CuTRZMoO_4$@PPy-n): PXRD pattern, (b) Raman spectra and (c) XPS spectra of $CuTRZMoO_4$@PPy-2; (d) C 1s; (e) N1s; (f) Cu 2p; (g) Mo 3d; (h) O 1s.

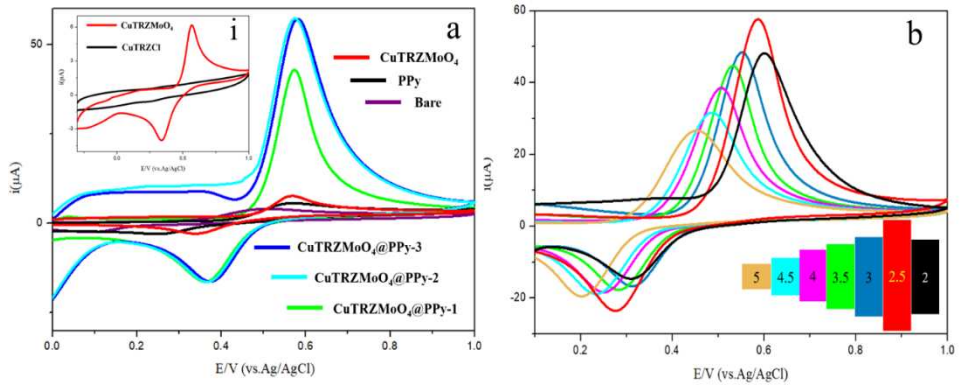

Fig. 3. (a) Cyclic voltammograms of different modified electrodes in 0.1 M PBS (pH 2.5) containing 0.2 mM DA at the scan rate of 50 mV s^{-1}, and the illustration (i) in panel a is the cyclic voltammetry of $CuTRZMoO_4$ and CuTRZCl. (b) CVs of $CuTRZMoO_4$@PPy-2/GCE in 0.1M PBS at different pH values (pH: 5.0, 4.5, 4.0, 3.5, 3.0, 2.5 and 2.0). Scan rate: 50mV s^{-1}. DA: 0.2 mM.

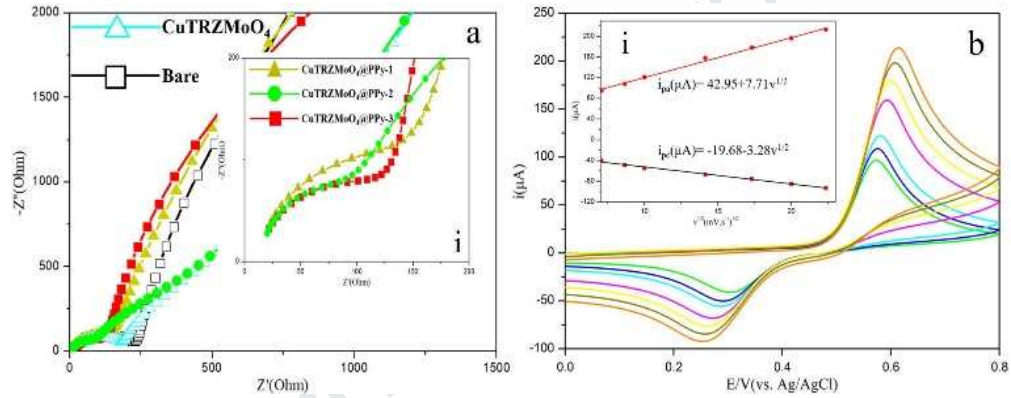

Fig. 4. (a) Nyquist plots of EIS of bare, CuTRZCl, $CuTRZMoO_4$, $CuTRZMoO_4$@PPy-1, $CuTRZMoO_4$@PPy-2 and $CuTRZMoO_4$@PPy-3 in a 5 mmol L^{-1} $[Fe(CN)_6]^{3-/4-}$ solution with 0.1 mol L^{-1} KCl. The insets in panel are related to (i) the close view of $CuTRZMoO_4$@PPy-1, $CuTRZMoO_4$@PPy-2 and $CuTRZMoO_4$@PPy-3 curve. (b) CV curves for 0.5 mM DA on $CuTRZMoO_4$@PPy-2 in 0.1 mol L^{-1} PBS solutions (pH 2.5) with different scan rates. The insets in panel b are (i) linear relationship between the cathodic or anodic peak currents and the square root of the scan rate.

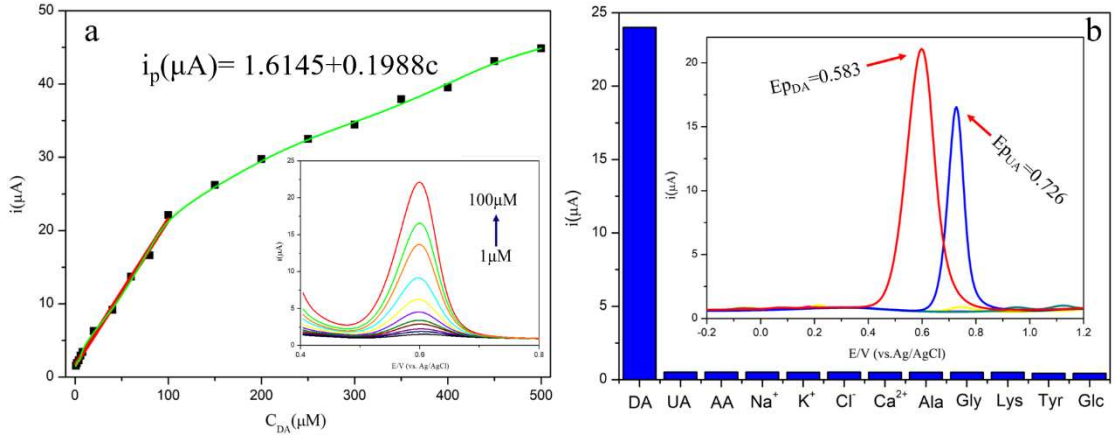

Fig. 5. (a) DPV curves for diμerent concentrations of DA (1-100 μmol L^{-1}) on $CuTRZMoO_4$@PPy-2 in 0.1 mol L^{-1} PBS (pH 2.5). (b) The selectivity of CuTRZMoO4@PPy-2/GCE electrode to DA. Each substance was added into reaction solution 0.1M PBS (pH=2.5). Various substances are DA, AA, UA, Na^+, K^+, Cl^-, Ca^{2+}, Ala, Gly, Lys, Tyr, and Glc. The concentration of DA and UA was 100 μmol L^{-1}, and the concentration of other potential interfering substances was 1000 μmol L^{-1}.

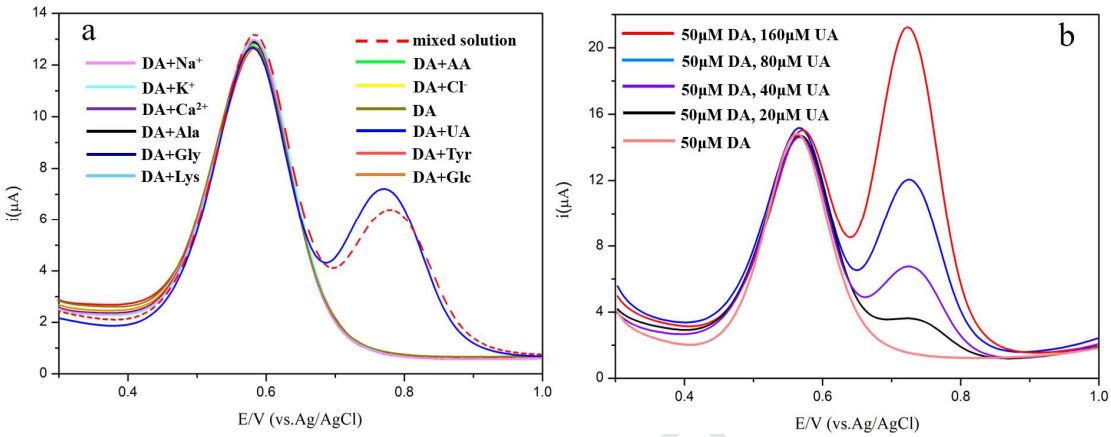

Fig. 6. (a) The current changes from adding different interferents and (b) the current changes from adding different concentrations of UA.

Highlights

1. Molybdenum oxide-based metal-organic framework ($[Cu_3(trz)_2(MoO_4)_2]\cdot H_2O$) were synthesized.
2. Adjusting the metal centers of Mo based MOFs and employing conductive PPy to dopamine (DA) detection is discussed.
3. The $CuTRZMoO_4$@PPy exhibit the excellent detection of DA with wide linear detection range (1-100 μM) and very low limit of detection (80 nM).

Notes

The authors declare no competing financial interest.